Comparison of FGO and KF for PDR-GNSS Fusion Under Different PDR Errors

Amjad Hussain Magsi and Luis Enrique Díez

***Abstract*— Smartphone-based positioning, heralded for its widespread accessibility, encounters challenges due to its reliance on global navigation satellite systems (GNSSs) in unfavorable conditions such as urban canyons, tunnels, and indoor areas. Even in clear-sky conditions, signal distortions, interruptions, and the limitations of cost-effective smartphone GNSS prompt researchers to explore alternative positioning methods. This has led to the adoption of sensor fusion techniques, often integrating the inertial measurement unit (IMU) for its complementary features with GNSS. In pedestrian localization, the fusion of pedestrian dead reckoning (PDR) and GNSS, traditionally employing the Kalman filter (KF) as the main fusion algorithm, has been standard practice. The emerging factor graph optimization (FGO) algorithm has recently gained attention for its better accuracy for inertial navigation system (INS)-GNSS fusion architectures, especially under GNSS outliers. However, the FGO implementation for PDR-GNSS fusion architecture has been less investigated, and little is known about its performance under different PDR outliers. As the different gait dynamics of humans and transient variations in the way the smartphone is carried, the PDR system can generate short and high errors (SHEs) or continuous and low errors (CLEs). We analyze the improvement of FGO over KF in mitigating these PDR errors in the PDR-GNSS fusion architectures for smartphone-based positioning. Since FGO is a smoothing technique and KF is a filtering method, for a fairer comparison, we also implemented a smoothed KF (SKF) using the Rauch–Tung–Striebel smoother (RTSS) technique. Our investigation, involving ten individuals with diverse heights, genders, and gait patterns in walking and running motions, underscores FGO's superior performance in the presence of PDR errors and across various pedestrian and motion scenarios, achieving a stable 25% improvement for the mean position error and 30% for the median position error in comparison to KF, 24% mean improvement, and 32% median improvement in comparison to SKF. Furthermore, the convergence time for FGO after the SHE PDR errors is comparably shorter than SKF and KF.**

***Index Terms*— Factor graph optimization (FGO), fusion, global navigation satellite system (GNSS), Kalman filter (KF), outliers, pedestrian, pedestrian dead reckoning (PDR), smartphone.**

I. Introduction

WITH the prevalence and accessibility of smartphones in today's digital age, pedestrian positioning has witnessed a substantial increase. Smartphones have become the predominant tools for individuals relying on positioning and localization services, with the global navigation satellite system (GNSS) playing a pivotal role in smartphone-based positioning, especially optimized for outdoor environments characterized by unobstructed views of the sky and direct satellite reception [1]. However, the performance of GNSS deteriorates in indoor environments such as tunnels and buildings, as well as in densely urban outdoor areas. In these scenarios, GNSS signals become weaker and susceptible to multipath interference and non-line-of-sight (NLOS) conditions, leading to noise issues and occasional data gaps in smartphone GNSS chips [2], [3], [4], [5]. To address this issue, researchers have focused more on alternative positioning solutions and have come up with the multisensor fusion concept in order to boost the performance of GNSS-based positioning in smartphones. Modern smartphones are equipped with a range of sensors that can serve as alternative positioning. These sensors include the camera, inertial sensors, barometer, light sensors, BLE, Wi-Fi, and even LiDAR. Among them, inertial sensors hold greater importance due to their complementary features with GNSS. They offer low short-term errors and are not susceptible to signal blockage caused by multipath interference or NLOS conditions. Furthermore, they do not necessitate additional infrastructure. This makes inertial + GNSS a well-known and popular fusion architecture [6], [7], [8]. However, this fusion can be implemented in several ways, depending on the different types of inertial navigation, GNSS processing techniques, the utilization of multiple constellations and frequencies, fusion algorithms, and integration levels, as depicted in the accompanying Fig. 1.

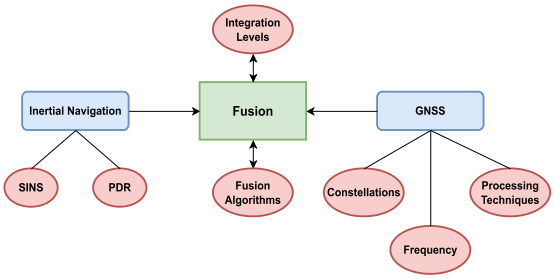

Fig. 1. Inertial-GNSS fusion architecture mechanism.

The high noise of the microelectromechanical systems (MEMSs) inertial measurement unit (IMU) present in smartphones makes the strapdown inertial navigation system (SINS) impractical due to the fast error accumulation over time. In addition, smartphone carrying modes do not allow

Manuscript received 1 January 2024; revised 14 June 2024; accepted 2 July 2024. Date of publication 12 August 2024; date of current version 26 August 2024. This work was supported in part by the Research Training Grants Program of the University of Deusto and in part by REPNIN++ under Grant RED2022-134355-T. The Associate Editor coordinating the review process was Dr. Martti Kirkko-Jaakkola. *(Corresponding author: Amjad Hussain Magsi.)*

The authors are with the Faculty of Engineering, University of Deusto, 48007 Bilbao, Spain (e-mail: amjad.hussain@deusto.es; luis.enrique.diez@deusto.es).

Digital Object Identifier 10.1109/TIM.2024.3440373

for the implementation of techniques such as zero velocity update (ZUPT) for reducing the error rate [9]. Pedestrian dead reckoning (PDR) is an alternative navigation method based on integrating each step displacement, reducing the error rate this way compared to pure inertial navigation system (INS). Consequently, the fusion of PDR and GNSS is a common architecture for pedestrian positioning using smartphones, which is still an open research topic [10], [11], [12], [13], [14]. In order to alleviate the errors of low-cost IMUs, PDR is based on detecting steps, estimating their length and direction, and then integrating the associated displacements to update the user's position. We can divide the errors associated with such detection and estimation processes into two types.

1) *Short and High Errors (SHEs):* Situations such as transient variations in the way the smartphone is carried can generate brief but large errors (outliers).
2) *Continuous and Low Errors (CLEs):* Human gait dynamics vary due to changes in walking pattern, gender, and height, and these factors influence the performance of individual PDR blocks, making it difficult to develop methods that generalize PDR performance for any user. This leads to CLEs in the PDR block.

To address this challenge, fusion algorithms play a crucial role in mitigating the impact of PDR errors for such fusion architectures. Historically, the Kalman filter (KF) has served as the primary fusion algorithm for the PDR-GNSS fusion architecture. However, achieving high accuracy using KF and its variant models has been challenging due to the linear first-order Markov dynamic model, Gaussian noise assumptions, and the fact that it considers only the latest available measurement. Instead, the newly proposed factor graph optimization (FGO) [15] is a well-liked approach for the multisensor fusion concept. Factor graphs are graphical models used to effectively address complex estimation problems such as simultaneous localization and mapping (SLAM) [16]. FGO optimizes state estimates through iterative solutions, treating state estimation as a nonlinear least-squares problem. It employs historical measurements and iterative solvers such as Gauss–Newton or Levenberg–Marquardt to minimize the cost function, achieving optimal estimations. Consequently, there is a growing trend to utilize FGO as an alternative to KF for both GNSS processing and inertial-GNSS fusion. Researchers [17], [18], [19], [20], [21], [22], [23] fused INS and GNSS using FGO and compared its performance against the traditional KF. Their findings highlighted FGO's notable capability to mitigate GNSS outliers, particularly in scenarios characterized by urban canyons or limited visibility of satellites during vehicular testing.

Up until now, there has been limited research on PDR-GNSS using FGO on smartphones. Past studies mainly focused on such fusion architectures for walking with smartphones and found that FGO outperformed traditional KF [10], [11], [12], [24], [25]. In the same way that some studies have explored the impact of GNSS outliers on FGO in INS-GNSS fusion, we believe that it is equally important to examine FGO's effect on PDR outliers, which occur more frequently than INS outliers. To the best of our knowledge, no one has yet investigated the impact of PDR errors on FGO performance. We compared FGO and KF in PDR-GNSS fusion for walking and running motions using a single dataset. Results showed that FGO performed better overall though its effectiveness slightly decreased during running compared to walking. In the running motion, the PDR's accuracy was affected due to misleading step detections and step length estimation compared to walking. This highlights a significant research gap in evaluating FGO against KF for various PDR errors stemming from diverse smartphone disturbances, multiple pedestrians with differing heights, genders, walking patterns, and distinct motions. In this extended version of our previous article [26], we highlight a deeper understanding of FGO's capabilities and limitations.

It is usually hard to generalize PDR performance to different users and motion modes. We aim to provide valuable insights into the effectiveness of fusion algorithms within the PDR-GNSS architecture, with a specific focus on their performance in PDR errors, i.e., various pedestrians, motions (CLE), and outliers (SHE). Since FGO is a smoothing technique and KF is a filtering method, for a fairer comparison, we also implemented a smoothed version of KF (SKF) using the Rauch–Tung–Striebel smoother (RTSS) technique [27]. We hypothesize that FGO deals with that better than KF and SKF.

The main contributions of this research are given as follows.

1) *Exploration of PDR Outliers:* We examined how FGO, SKF, and KF performed under various PDR outliers (SHEs), which are caused by different disturbances to smartphone carrying, which produce a negative influence on the PDR accuracy. FGO's effectiveness in handling these PDR outliers is analyzed, as it has been done similarly in the literature to assess the impact of GNSS outliers for INS-GNSS.
2) *Analysis of Different Pedestrians and Motions With FGO:* The performance of the PDR block is impacted by pedestrians with varying heights, walking patterns, and genders. To scrutinize the associated PDR errors (continuous and long errors) stemming from diverse pedestrian characteristics and movements, we examined multiple individuals of varying heights and genders engaged in both running and walking activities. Our analysis aimed to evaluate the effectiveness of FGO compared to KF in mitigating these PDR errors associated with the lack of generalization ability.

The remaining article is structured as follows. Section II provides an overview of the related work. Section III presents the proposed methodology, which includes the development of the PDR mechanism and the development of KF- and FGO-based PDR-GNSS fusion architectures. Section IV describes the experimental evaluation and setup. Section V details the results. Finally, Section VI concludes this article, summarizing the findings and future work.

II. Related Work

A. Traditional PDR-GNSS Fusion Approaches

PDR is a widely recognized inertial navigation algorithm designed for pedestrians that works on three fundamental aspects: step detection, step length estimation, and step heading estimation. These displacement-related parameters are usually obtained from data provided by inertial sensors such as accelerometers and gyroscopes. PDR, on its own, tends to accumulate position errors over time, mainly due to variations in pedestrian walking patterns. Therefore, enhancing localization accuracy necessitates integration with GNSS. Many researchers have already explored PDR-GNSS fusion architectures [13], [28], [29], [30]. [28] proposed the PDR-GNSS fusion method by jointly estimating the heading angle and step length. However, they did not account for the negative influence of GNSS MP and NLOS signal reception. Therefore, later on, Rehman et al. [13] focused on the MP and NLOS conditions, and with this, they addressed the issue of cumulative errors stemming from the estimation of heading and step size. They mitigate these errors by implementing metrics for mean cumulative heading error and cumulative step length error, respectively. Following this error reduction process, they integrate PDR with GNSS to enhance the overall performance. Another study [29] introduced a precise displacement estimation method by integrating PDR and GNSS using a time-differenced carrier phase (TDCP). The TDCP-PDR-GNSS integration approach demonstrated a significant reduction in position errors, thereby improving the accuracy of the estimated displacements. The optimization-based PDR (OBPDR) was proposed [30] through an improved finite state machine (IFSM) gait detection method. Then, they fused this OBPDR with GNSS for better results.

B. FGO-Based PDR-GNSS Fusion Architecture

The traditional fusion approaches have several issues that have been highlighted by [31]. These issues are summarized as follows.

1) Traditional single-source navigation methods lack efficiency, while integrated systems, which emphasize specific sensors and measurements, limit adaptability and precision.
2) System miniaturization and clustering introduce nonlinear and non-Gaussian challenges in navigation, exceeding traditional filtering methods' precision capabilities.
3) The navigation system faces sensor data synchronization challenges, held back by sensor heterogeneity and varying working conditions, making traditional alignment methods inadequate.

To address these issues, the USA-based Advanced Defense Research Project Agency (DARPA) introduced the concept of all-source positioning and navigation (ASPN) in November 2010. ASPN proposes to merge data sources for versatile navigation, featuring quick integration and adaptability. However, practical implementation remains challenging. Georgia Institute of Technology came up with the concept of factor graph-based methods and made early attempts with this for ASPN. Factor graph-based methods, known for plug-and-play functionality and the ability to handle complex, asynchronous data, have gained recent attention [32].

The introduction of the FGO formulation by Indelman et al. [33] has paved the way for a fresh perspective on multisensor integration, as further explored by [34] and [35]. The factor graph improves state estimation by considering past measurements and system updates. Unlike the KF, FGO iteratively adjusts the measurement model, enhancing accuracy. Factor graphs efficiently use time correlations between past and present data through batch-style processing. In this mode, a factor graph acts as both a forward filter and a backward smoother after each measurement update. Thus, FGO is applied in demanding GNSS situations, as highlighted in works by [36], [37], [38], [39], and [40]. Furthermore, Pfeifer and Protzel [41] illustrated FGO's significant promise in sensor fusion, even when dealing with non-Gaussian noise models. Researchers have recently worked on the fusion of INS and GNSS for vehicular navigation systems, in which they fused the professional inertial and GNSS devices [18], [19], [42], [43], [44].

In the context of pedestrian navigation using a smartphone, a relatively limited body of research exists. Only a handful of researchers have explored the fusion of PDR and GNSS for smartphones. Jiang et al.'s [10], [11] research team was the first one proposing FGO-based PDR-GNSS fusion: In [10], they delved into the performance and implementation of FGO compared to KF for single-user and walking motion data only, in which they showed that FGO is better than KF. Later, in [11], they proposed two modifications by introducing two constraints (position and distance) in the factor graph and evaluated the performance against KF using multiple datasets collected in open sky and partially open sky conditions by placing the smartphone handheld and in a backpack and pocket for only walking motion. They also proposed a cooperative positioning system based on FGO PDR-GNSS fusion [24]. More recently, they proposed a tight-coupled FGO PDR-GNSS fusion-based [25]. They employed fuzzy adaptive FGO to further enhance accuracy and suppress pseudorange outliers. In a similar work, Zhong et al. [12] investigated the tightly coupled FGO-based PDR-GNSS fusion for urban canyons in which they created the factor graph constraints from raw GNSS pseudorange, Doppler measurements, and raw accelerometer-based PDR algorithm. They also proposed smoothness-driven motion model-based pedestrian navigation with a small acceleration for trajectory smoothing and increased resilience to potential GNSS outliers in standalone positioning.

In the above studies, the authors have primarily focused on the quality of the fused solution and the impact of the GNSS outliers, considering only walking motion. However, to the best of our knowledge, no one has yet examined the impact of PDR errors caused by various human motions, different gait patterns, and transient variations in smartphone positioning. In our previous article [26], we highlighted the performance of FGO for walking and running motion using a single user. Each pedestrian has a unique walking style, influenced by factors such as height, gender, body posture, and dynamics. The results revealed FGO's superiority in both motions, but, still, there is a need to investigate FGO's performance with different

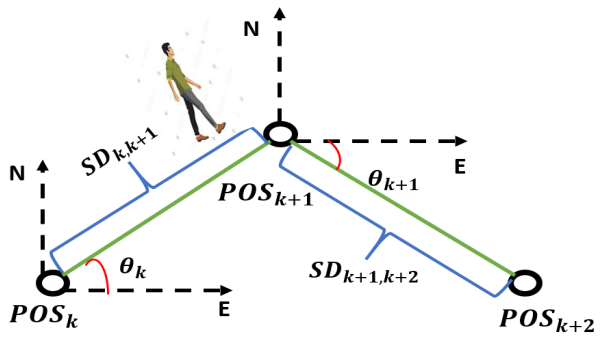

Fig. 2. PDR mechanism.

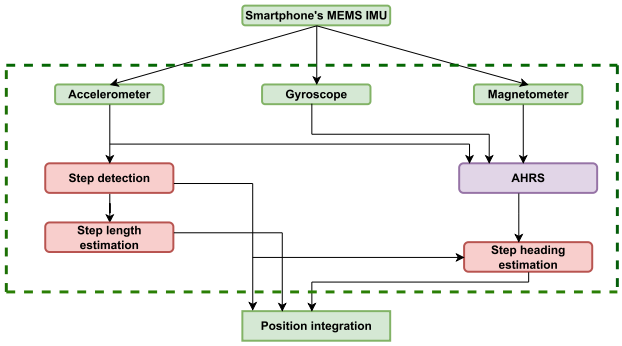

Fig. 3. Smartphone-based PDR.

aspects of PDR errors. Second, due to transient variations in smartphone position from normal placement to sudden, rapid changes that can lead to misdetected steps and heading errors, this article aims to analyze the FGO performance under PDR outliers (SHEs), in the same fashion as other works studied the impact of GNSS outliers for both PDR-GNSS and INS-GNSS [19].

III. Methodology

In this section of this article, we elaborate on the methodological approach adopted in this study, which includes the development of PDR and its fusion with GNSS through both the KF and FGO techniques.

A. Development of PDR

PDR estimates pedestrian movements based on the detection of steps, step length, and heading estimation. The PDR working mechanism shown in Fig. 2 can be mathematically written as follows:

$$\mathbf{Pos}_{k+1} = \mathbf{Pos}_k + \Delta\mathbf{Pos}_{k|k+1} \tag{1}$$

where $\mathbf{Pos}_{k+1}$ and $\mathbf{Pos}_k$ represent the position at steps $k+1$ and k, respectively, and $\Delta\mathbf{Pos}_{k|k+1}$ represents the position increment from step k to $k+1$ that, expressed in the east north up (ENU) reference system [9], can be written as

$$\Delta\mathbf{Pos}_{k|k+1} = \begin{bmatrix} \Delta\mathbf{Pos}^E_{k|k+1} \\ \Delta\mathbf{Pos}^N_{k|k+1} \end{bmatrix} = \begin{bmatrix} \mathbf{SL}_{k|k+1} \cdot \cos(\phi) \\ \mathbf{SL}_{k|k+1} \cdot \sin(\phi) \end{bmatrix} \tag{2}$$

where the heading angle is indicated by ϕ and the step length from step k to step $k+1$ is shown by $\mathrm{SL}_{k|k+1}$.

A schematic illustration of the PDR system from the smartphone is presented in Fig. 3. For step detection, we utilized the magnitude of the triaxial accelerometer [see (3)] as an input signal. To detect steps, we used the code provided by [10], and we modified some threshold values to adapt the step detector to different motion modes

$$|\mathrm{Acc}_k| = \sqrt{\mathrm{Acc}^2_{xk} + \mathrm{Acc}^2_{yk} + \mathrm{Acc}^2_{zk}}. \tag{3}$$

For step length estimation, we employed Weinberg's algorithm [45]; within each detected step, the step length is determined from the range of the acceleration magnitude values and a scaling constant factor

$$\mathrm{SL}_{k|k+1} = C \cdot [\max(|\mathrm{Acc}_k|) - \min(|\mathrm{Acc}_k|)]^{1/4} \tag{4}$$

where $\mathrm{SL}_{k|k+1}$ represents the estimated step length between two consecutive acceleration peaks and C is a constant factor used to scale the estimated step length.

For step heading estimation, we employed the heading angle obtained from the attitude and heading reference system (AHRS) integrated into the smartphone at each detected step epoch.

B. KF-Based PDR-GNSS Fusion Architecture in Smartphone

The KF operates through two steps: the prediction step and the correction step. In the prediction step, the state of the system at the next time step is estimated by using a dynamic model and the current state of the system. The correction step, on the other hand, involves refining the estimated state by incorporating measurements from sensors. This allows for an update of the estimated state, resulting in a more accurate position estimation. The state vector, represented as $\mathbf{X}$, serves as the fundamental element for the state transformation in PDR-GNSS integration, which is the position errors of PDR in x- and y-coordinates. Therefore, we have implemented a KF-based fusion using an error state approach instead of a position state, which is based on a linear dynamic model as outlined by [10] and [11]

$$\mathbf{X} = \begin{pmatrix} \Delta\mathrm{PDR}_x \\ \Delta\mathrm{PDR}_y \end{pmatrix}.$$

The formulation of this transformation is expressed as follows:

$$\mathbf{X}_{k+1} = \mathbf{F}_{k|k+1} \cdot \mathbf{X}_k + \mathbf{W}_{k+1} \tag{5}$$

where $\mathbf{X}_{k+1}$ and $\mathbf{X}_k$ indicate the state vector at $k+1$ and k epochs, respectively; $\mathbf{W}_{k+1}$ is a process noise vector, which is assumed to be subject to a standard Gaussian distribution, expressed as $\mathbf{W}_{k+1} \sim \mathcal{N}(0, Q_k)$, where Q_k represents the covariance matrix of the process noise and $\mathbf{F}_{k|k+1}$ refers to the transformation matrix at epochs $k+1$ and k

$$\mathbf{F}_{k|k+1} = \begin{bmatrix} 1 & 0 \\ 0 & 1 \end{bmatrix}. \tag{6}$$

The measurement model is

$$\mathbf{Z}_{k+1} = \mathbf{H}_{k+1} \cdot \mathbf{X}_{k+1} + \mathbf{V}_{k+1}. \tag{7}$$

Equation (7) represents the general measurement model, combining the state vector $\mathbf{X}_{k+1}$, observation matrix $\mathbf{H}_{k+1}$, and measurement noise vector $\mathbf{V}_{k+1}$ to calculate the predicted measurement $\mathbf{Z}_{k+1}$. The actual observations are calculated

differently in the following equation, specifically tailored for our PDR-GNSS fusion approach:

$$\mathbf{Z}_{k+1} = \mathbf{Pos}_{k+1}^{\mathrm{GNSS}} - \mathbf{Pos}_{k+1}^{\mathrm{PDR}}. \tag{8}$$

In this equation, the actual observations $\mathbf{Z}_{k+1}$ are derived as the difference between the GNSS position estimate $\mathbf{Pos}_{k+1}^{\mathrm{GNSS}}$ and the PDR position estimate $\mathbf{Pos}_{k+1}^{\mathrm{PDR}}$ at time $k+1$. Also, the $\boldsymbol{H}_{k+1}$ observation matrix can be written as follows:

$$\boldsymbol{H}_{k+1} = \begin{bmatrix} 1 & 0 \\ 0 & 1 \end{bmatrix}. \tag{9}$$

The prediction step of KF can be mathematically written as follows:

$$\mathbf{X}_{k+1}^{-} = \mathbf{F}_{k|k+1} \cdot \mathbf{X}_k \tag{10}$$

$$\mathbf{P}_{k+1}^{-} = \mathbf{F}_{k|k+1} \cdot \mathbf{P}_k \cdot \left(\mathbf{F}_{k|k+1}\right)^{\mathrm{T}} + \mathbf{Q}_k. \tag{11}$$

In these equations, $\mathbf{X}_{k+1}^{-}$ and $\mathbf{P}_{k+1}^{-}$ are the a priori estimated state vector and covariance matrix, respectively, obtained by applying the dynamic model to the previous estimation. Then, the correction step for KF updates the state estimation as follows:

$$\hat{\mathbf{X}}_{k+1} = \mathbf{X}_{k+1}^{-} + \mathbf{K}_{k+1} \cdot \left(\mathbf{Z}_{k+1} - \mathbf{H}_{k+1} \cdot \mathbf{X}_{k+1}^{-}\right) \tag{12}$$

$$\mathbf{K}_{k+1} = \mathbf{P}_{k+1}^{-} \cdot (\mathbf{H}_{k+1})^{\mathrm{T}} \cdot \left[\mathbf{H}_{k+1} \cdot \mathbf{P}_{k+1}^{-} \cdot (\mathbf{H}_{k+1})^{\mathrm{T}} + \mathbf{R}_{k+1}\right]^{-1} \tag{13}$$

$$\mathbf{P}_{k+1} = (\mathbf{I}_{2\times 2} - \mathbf{K}_{k+1} \cdot \mathbf{H}_{k+1}) \cdot \mathbf{P}_{k+1}^{-} \tag{14}$$

where $\hat{\mathbf{X}}_{k+1}$ is the updated state estimation at $k+1$, $\mathbf{K}_{k+1}$ represents the Kalman gain matrix at $k+1$, and $\mathbf{I}_{2\times 2}$ represents the identity matrix of size 2×2.

C. Implementation of the SKF Using RTSS

As the KF is a forward filtering method that does not consider historical measurements, we employed the RTSS technique to implement the SKF [27]. This allows for a more equitable comparison with FGO, which is inherently a smoothing technique. The SKF implementation involved the following steps.

1) Forward Pass (KF): Estimation of the state variables using the standard KF equations, as described above.

2) Backward Pass (RTSS): Smoothing the state estimates using the RTSS equations. The RTSS algorithm involves a backward recursion that refines the forward pass estimates by considering future measurements, leading to more accurate state estimates.

The RTSS equations are given as follows.

Smoothing Gain:

$$G_k = P_{k|k} A^{\mathrm{T}} P_{k+1|k}^{-1}. \tag{15}$$

Smoothed State:

$$\hat{x}_{k|N} = \hat{x}_{k|k} + G_k\left(\hat{x}_{k+1|N} - \hat{x}_{k+1|k}\right). \tag{16}$$

Smoothed Covariance:

$$P_{k|N} = P_{k|k} + G_k\left(P_{k+1|N} - P_{k+1|k}\right)G_k^{\mathrm{T}}. \tag{17}$$

In these equations, $\hat{x}_{k|N}$ represents the smoothed state estimate at time k given all measurements up to time N, $P_{k|N}$ is the smoothed covariance matrix, and G_k is the smoothing gain that adjusts the state estimate based on future observations.

3) Smoothing Factor: The term "smoothing factor" refers to the parameters influencing the RTSS process. In our implementation, these include the following.

1) *Process Noise Covariance (Q_k):* Tuned to reflect the variability and dynamics of pedestrian movement.
2) *Measurement Noise Covariance (R_k):* Determined based on the expected accuracy of GNSS and PDR measurements.
3) *State Initialization:* Initial state estimates and their covariances were carefully chosen to ensure stability and convergence of the smoother. These factors collectively determine the effectiveness of the smoothing process. For pedestrian navigation, the process and measurement of noise covariances were specifically tuned through empirical analysis to handle the variations in human gait and smartphone handling. Moreover, these noise covariances are listed under fusion method parameterization in Section IV.

D. FGO-Based PDR-GNSS Fusion Architecture in Smartphone

A factor graph is a probability model that utilizes a graph to represent the probability dependence of different variables. Specifically, a factor graph is a bipartite graph composed of two types of nodes: the unknown state variables and the factor nodes, which represent the conditional probabilities of some set of state variables. The undirected edges connect the state variable nodes and corresponding factor nodes. There is an edge between the two nodes only when the variable node and the factor node have a functional relationship. A factor graph allows the decomposition of a global probability function into the product of multiple local probability functions, reducing the complexity of solving the global function.

In sensor integration, we are usually interested in estimating a set of state variables X from a set of given measurements Z. Assuming a Markov model, that conditional probability density function can be formulated

$$P(X|Z) = \prod_{i=1}^{k} \frac{P(z_i|x_i)P(x_i|x_{i-1}, u_i)}{P(z_i)} P(x_0) \tag{18}$$

where z_i represents the measurements observed at epoch i (e.g., GNSS measurements), x_i represents the system state at i, and u_i denotes the control input (e.g., PDR measurements).

The most often used estimator for these unknown state variables X is the maximum a posteriori or MAP estimate

$$\hat{X} = \arg\max P(X|Z) = \arg\max \prod_{i=1}^{k} P(z_i|x_i)P(x_i|x_{i-1}, u_i). \tag{19}$$

In FGO-based integration, all these likelihood and transition probabilities are treated as the factorization of the global probability

$$\hat{X} = \arg\max \prod_{j=1}^{n} f\left(x_j\right). \tag{20}$$

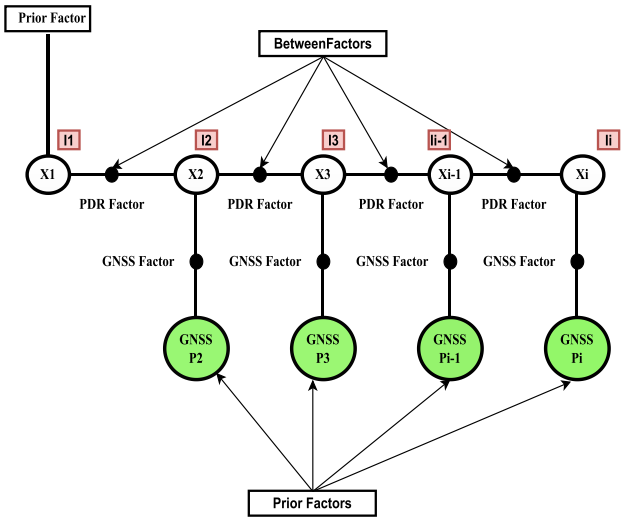

Fig. 4. Formation of PDR and GNSS factors within FGO mechanism.

Each factor models a constraint and must include a measure of uncertainty. The most common model is Gaussian noise

$$P(z_i|x_i) \propto \exp\left(-\frac{1}{2}\|h_i(x_i - z_i)\|^2 \nabla_i\right) \tag{21}$$

$$P(xi|x_{i-1}) \propto \exp\left(-\frac{1}{2}\|\Phi_i(x_{i-1} - x_i)\|^2 \Omega_i\right) \tag{22}$$

where the function $\Phi_i(\cdot)$ describes the relationship between the preceding states x_{i-1} and x_i, the function $h_i(\cdot)$ represents the relationship between the state x_i and the measurement z_i, and the covariance matrices are denoted by ∇_i and Ω_i.

Taking the negative log and dropping the factor $1/2$ transform the problem into the minimization of an error function, that is, a nonlinear least-squares problem

$$\hat{X} = \arg\min\left(\sum_{i=1}^{k} \|\Phi_i(x_{i-1}) - x_i\|^2_{\Omega_i} + \sum_{i=1}^{k} \|h_i(x_i) - z_i\|^2_{\nabla_i}\right). \tag{23}$$

In our case, as shown in Fig. 4, the factors represent the GNSS measurements and the transition between states due to the motion model and PDR measurements.

1) PDR Factor: This factor signifies the constraint enforced by the motion model derived from the PDR system. As can be seen, the PDR factor is modeled using the true-state nonlinear dynamic model, in contrast to the error-state linear dynamic model used in the KF implementation. This way, the potential advantage of the FGO dealing with nonlinear models is counteracted. This strategy was also followed by [10], [11], and [12]

$$\begin{aligned}\left\|e^{\text{PDR}}_{k+1}\right\|^2_{\sum^{\text{PDR}}_{k+1}} &= \|X_{k+1} - f(X_k)\|^2_{\sum^{\text{PDR}}_{k+1}} \\ &= \left\|x_{k+1} - \left(x_k + \begin{bmatrix}\mathbf{SL}_{t,t+1} \cdot \cos(\phi) \\ \mathbf{SL}_{t,t+1} \cdot \sin(\phi)\end{bmatrix}\right)\right\|^2_{\sum^{\text{PDR}}_{k+1}}.\end{aligned} \tag{24}$$

2) GNSS Factor: Similarly, this factor represents the constraint imposed by the GNSS measurements

$$\left\|e^{\text{GNSS}}_{k+1}\right\|^2_{\sum^{\text{GNSS}}_{k+1}} = \|X_{k+1} - \text{GNSS}_{k+1}\|^2_{\sum^{\text{GNSS}}_{k+1}}. \tag{25}$$

Therefore,

$$\hat{X} = \arg\min\left(\sum_{i=1}^{k}\left[\left\|e^{\text{PDR}}_{i+1}\right\|^2_{\sum^{\text{PDR}}_{i+1}} + \left\|e^{\text{GNSS}}_{i+1}\right\|^2_{\sum^{\text{GNSS}}_{i+1}}\right]\right). \tag{26}$$

We utilized the Georgia Tech Smoothing and Mapping (GTSAM) library, an open-source tool developed by researchers at the Georgia Institute of Technology, to implement FGO [32]. This library is well-known for its effectiveness in solving problems related to SLAM, factor graphs, and pose graph-based optimization, making it user-friendly for FGO implementation in various applications. As mentioned before, the graph consists of PDR and GNSS factors. Whenever a new GNSS measurement is available, new PDR and GNSS factors are appended to the graph. After that, the Levenberg–Marquardt optimizer [46] is used to optimize the completely new graph, and this process is repeated after each new GNSS measurement. It is important to mention that other optimizers such as Newton–Gaussian, iSAM, and iSAM2 are also viable alternatives.

IV. Experimental Evaluation

A. Experimental Description

It is challenging to develop a flexible PDR for different pedestrian walking patterns and various carrying modes of smartphones. We conducted two different experiments for SHE and CLE analyses.

For the SHE analysis, the experiment was conducted in an outdoor area with enough satellite visibility. The pedestrian held the smartphone initially aligned with its body and just walked at a normal pace for about 52 m on a predefined straight path, but while walking, the pedestrian moved his smartphone to generate short unexpected dynamics (outliers) as follows.

1) *Swinging of a Smartphone (Case I):* The smartphone briefly entered a swinging mode for a few seconds before returning to its original position.
2) *Changing the Heading of a Smartphone (Case II):* When changing the smartphone's heading, it was rotated counterclockwise for a few seconds twice along the entire path to observe outliers more clearly.
3) *Shaking of Smartphone (Case III):* Similarly, the smartphone was shaken in an upright position for a brief duration.

In another experiment aimed at observing CLE analysis across various pedestrians and motions (walking and running), participants completed a full lap along a predefined trajectory outdoors. Throughout the entire duration, each pedestrian held the smartphone in front of their chest. Participants were instructed to walk and run at their own natural pace while maintaining the same position of the smartphone.

B. Data Collection and Processing

The Huawei Y8P smartphone was used for inertial sensors and GNSS data. For reference, the Ublox ANN-MB-00-00

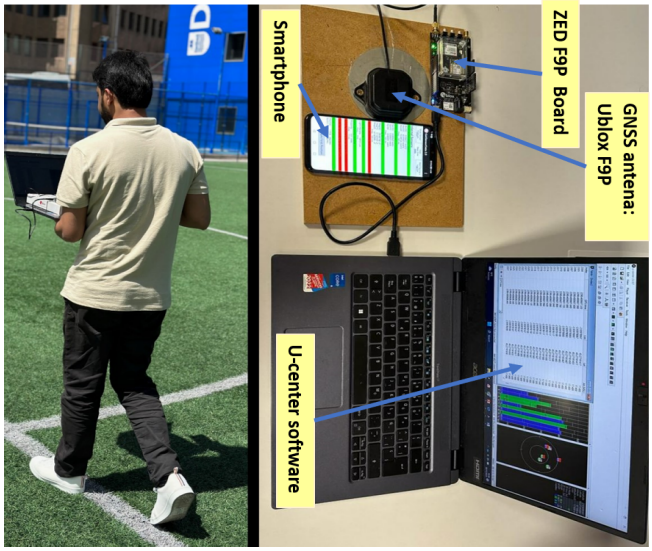

Fig. 5. Data collection and experimental setup.

TABLE I
DIFFERENT PEDESTRIANS FOR DATA COLLECTION

Pedestrian	Height (cm)	Gender	Pace
A	155 cm	Female	Own Will
B	160 cm	Male	
C	157 cm	Male	
D	150 cm	Male	
E	147 cm	Female	
F	140 cm	Female	
G	180 cm	Male	
H	185 cm	Male	
I	188 cm	Male	
J	168 cm	Male	

L1/L2 multiband GNSS antenna, which has a C099 F9P application processing board, has been used. Data collection took place outdoors in the open sky at the football field of the University of Deusto, Bilbao, Spain. We selected a small section of a straight-line path, spanning over 52 m. Refer to Fig. 5 for a visual representation of the data collection and experimental setup.

1) Smartphone Data: The GetSensorsData app [47] was used to collect inertial sensors and GNSS data from the smartphone.

The SHE analysis experiment involved three datasets, including smartphone swinging, heading change, and shaking. For the CLE analysis experiment, 40 datasets were collected from ten pedestrians with diverse heights, walking patterns, and genders, as detailed in Table I, encompassing both walking and running motions. Pedestrians had the flexibility to choose their own walking pace during the experiments. However, we set the upper threshold values for walking and running motions in the step detector.

2) Reference Data: The data were collected using U-Center 23.08 software provided by Ublox. The GPS, GLONASS, Galileo, and BeiDou satellite constellations were used to ensure the accuracy of the reference. The combined use of these satellite constellations resulted in a horizontal position accuracy of 2.5 cm.

3) Timely Synchronization of Reference and Smartphone Data: Every pedestrian, motion, and PDR outliers experiment has its own reference data, which has been synchronized with the smartphone via GPS time. We placed the Huawei Y8P smartphone's GNSS receiver right next to the reference data source (Ublox GNSS receiver), keeping the distance between them at 0 m. This proximity minimized any potential delays in the signals' travel, ensuring that our data were as precise as possible.

4) Fusion Methods' Parameterization: The efficacy of the FGO and KF fusion algorithms hinges on their adept utilization of parameter covariance settings. Throughout this study, we preserved uniform parameter settings for all pedestrian motions across the comprehensive dataset comprising 40 instances. Regarding the KF, we set the KF parameters as follows when we parameterize it in our case:

$$P = \begin{bmatrix} 0 & 0 \\ 0 & 0 \end{bmatrix}, \quad Q_k = \begin{bmatrix} 1 & 0 \\ 0 & 1 \end{bmatrix}, \quad R = \begin{bmatrix} 2 & 0 \\ 0 & 2 \end{bmatrix}$$

where P is the initial state covariance matrix, Q_k is the process noise covariance matrix, and R is the measurement noise covariance matrix.

In the domain of FGO, our approach involves two factors: PDR and GNSS. It is important to recognize that both of these factors come with uncertainties and noise. To handle these uncertainties, we have used GTSAM's odometry and prior noise model classes. We set the same values for both KF and FGO

$$\begin{aligned} &\text{odometryNoise} \\ &\quad = \text{noiseModel.Diagonal.Sigmas}([2;\ 2;\ 0.1]) \\ &\text{priorNoise} = \text{noiseModel.Diagonal.Sigmas}([1.4;\ 1.4;\ 0.1]). \end{aligned}$$

V. RESULTS

A. Analysis of Improvement in FGO Versus PDR Outliers

To characterize FGO performance over KF and SKF with transient variations in the way the smartphone is carried while walking, we fluctuated the smartphone during carrying in three different ways: swinging, changing the heading, and shaking the smartphone. From Figs. 6–8, it can be seen that with little disturbance, smartphone placement produces short-term high errors in the PDR models. We fused these PDR's displacements with GNSS using FGO and KF. In addition, we used SKF to make the comparison with FGO fair. The results indicated that FGO performed better than KF and SKF in all three cases.

Case I: In the case of smartphone swinging, Fig. 6(a) illustrates the noticeable impact on PDR output, evident in red as the PDR trajectory. The swinging of the smartphone not only produced general positional error but also the heading of the smartphone was changed, and the misdetection of the steps generated outliers in the PDR output, as visualized in Fig. 6(a). As a result, the PDR trajectory lost its path during swinging, leading to heightened positional errors over time, as portrayed in Fig. 6(c) and highlighted in purple. In comparison, the smartphone's GNSS remained stable, offering a contrast to

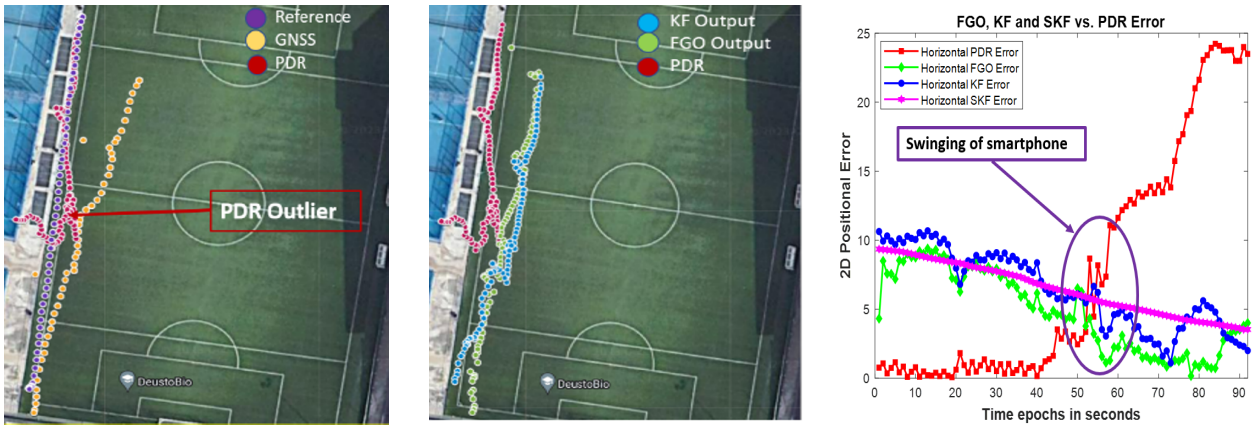

Fig. 6. (a) Reference, PDR output and GNSS trajectories are shown along with the effect of smartphone swinging on PDR's output highlighted in red. (b) Fused trajectories from KF and FGO, showing FGO's superior performance during smartphone swinging, outperforming KF. (c) Visualizes the horizontal position errors over time and reveals FGO's ability to mitigate PDR errors during smartphone swinging.

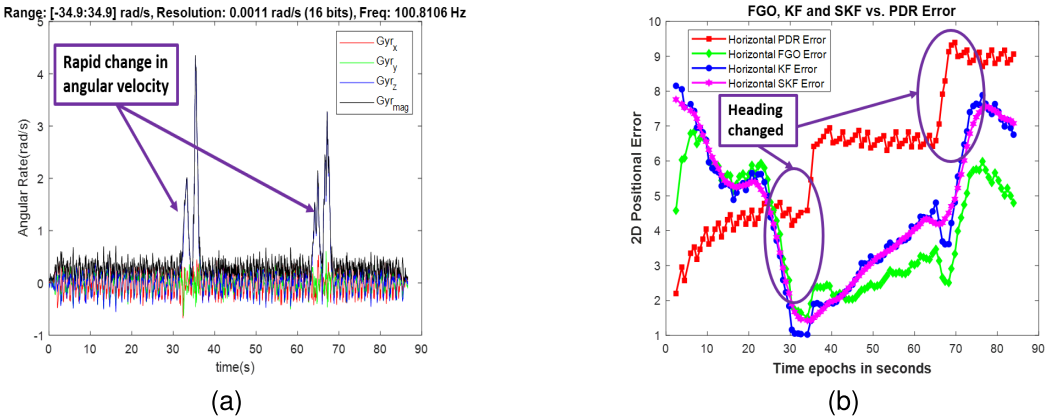

Fig. 7. (a) Rapid changes in the angular velocity when the smartphone was rotated. (b) Comparison of horizontal position errors from PDR, KF, SKF, and FGO with smartphone heading change (highlighted in purple).

the PDR's fluctuations. The fused trajectories from KF and FGO are shown in Fig. 6(b). It can be also seen that FGO is more robust to such high PDR error and produces better output especially when the PDR errors become so high. We computed the stable convergence time for these fusion techniques by setting the PDR error threshold at 10 m, which is when the errors peaked. We then observed how FGO, KF, and SKF responded to these outliers. The convergence time for FGO was 1.45 s compared to 3.78 s for KF and 5.36 s for SKF. This is due to the nature of FGO using historical measurements in an iterative process that helps it mitigate the impact of PDR errors in PDR-GNSS fusion architecture. Besides this, we set a fair comparison and implemented the SKF for fusion and compared it to FGO, which still shows the FGO superior to SKF, as well as emphasizing its enhanced performance in challenging conditions that can be seen in the comparison of SKF, KF, and FGO horizontal position errors over time [see Fig. 6(c)].

Case II: Similarly, we checked the FGO improvement when the smartphone heading changes during the walking motion. In Fig. 7, we present the horizontal position errors over time for PDR, KF, SKF, and FGO, as well as the angular rate over time. From Fig. 7(a), it can be seen that the angular rate was rapidly disturbed twice, and as a result, the effect in the PDR model can be seen in Fig. 7(b) highlighted in purple color.

Moreover, the improvement in FGO performance is greater compared to the first outlier, as FGO considers the historical measurements in the graph and then optimizes the whole graph. After the first PDR outlier, we set the PDR error threshold at 5 m, the point of peak error, to evaluate the convergence time for FGO, KF, and SKF. In this window, FGO took 1.90 s, KF 1.68 s, and SKF 1.70 s to converge post the first outlier. In the second outlier, FGO's convergence was slightly faster than SKF and KF. With a 7-m PDR error threshold, FGO converged in 3.14 s, KF in 4.20 s, and SKF in 4.24 s. It becomes more stable when it utilizes more historical measurements and optimizes the trajectory compared to KF and SKF, which works only on the last measurement and whose performance has degraded in the presence of second PDR outliers.

Case III: Similarly, in Fig. 8, when the smartphone experienced shaking, both step detection and heading were adversely affected, leading to inaccurate readings and high PDR horizontal errors over time. Following the smartphone shake, the PDR lost its trajectory and produced elevated errors that can be easily seen in Fig. 8(b). Despite encountering these challenges in the PDR block, the fused output generated by FGO demonstrated significantly improved results, effectively reducing errors and mitigating the impact of PDR errors. As highlighted in Fig. 8 with a purple color, it is noteworthy

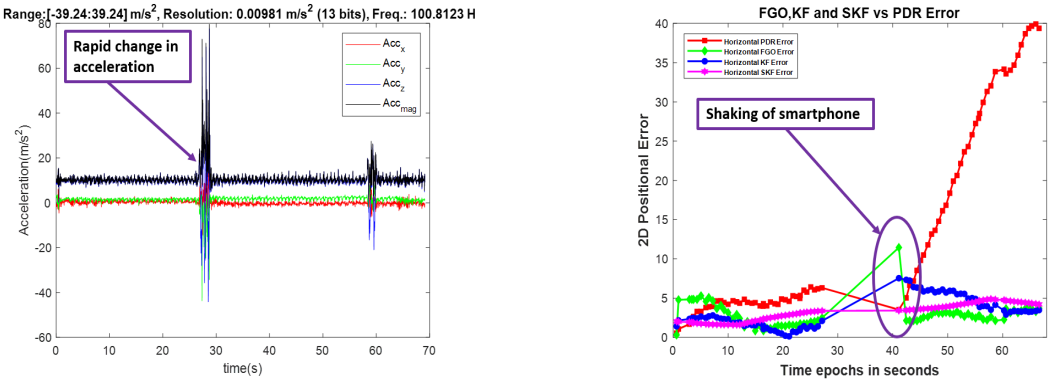

Fig. 8. (a) Rapid change in acceleration when the smartphone was shaken. (b) Comparison of horizontal position errors from PDR, KF, SKF, and FGO with smartphone shaking (highlighted in purple).

that during the shaking event, FGO's errors initially increased. However, immediately after the shaking, FGO swiftly reduced the errors, surpassing KF in error reduction. To determine the stable convergence time for FGO, KF, and SKF following the PDR outlier, we set the PDR error threshold at 11 m, which is when the errors peaked. Within this time window, the convergence time for FGO to address the PDR effect was 2.57 s, while, for KF, it was 5.58 s, and for SKF, it was 3.63 s. This observation underscores FGO's superiority over KF and SKF, even in the face of PDR errors.

The general implementation of the PDR model does not fit well with different carrying modes of smartphones. From the results, it can be seen that a disturbance of short duration in the smartphone's carrying style while walking produces a short-term and higher error in the PDR output, and eventually, the fusion methods produce lower errors while mitigating the bad performance of PDR models. However, the FGO seems like a better option compared to KF because it has fewer errors. Moreover, we have seen that FGO is more robust in mitigating the effect of PDR outliers in the same way as it has been analyzed that it mitigates the impact of GNSS outliers in the INS-GNSS fusion by [19]. Since FGO utilizes both current and previous measurements iteratively, each time a new measurement becomes available, FGO optimizes the entire factor graph. Therefore, it produces better output than SKF and KF. On the other hand, SKF also incorporates historical measurements. However, it is less robust compared to FGO due to its noniterative optimization approach, whereas KF only estimates based on the current and last measurements. To check the overall performance of FGO under the SHE PDR errors, the cumulative distribution function (cdf) and box plots of horizontal positioning errors obtained from three methods have been computed, and based on these analyses, FGO seems to be a better option than SKF and KF, which can be seen in Figs. 9 and 10. Moreover, from all three cases, it can be noted that FGO has a quicker convergence time to stability compared to KF and SKF.

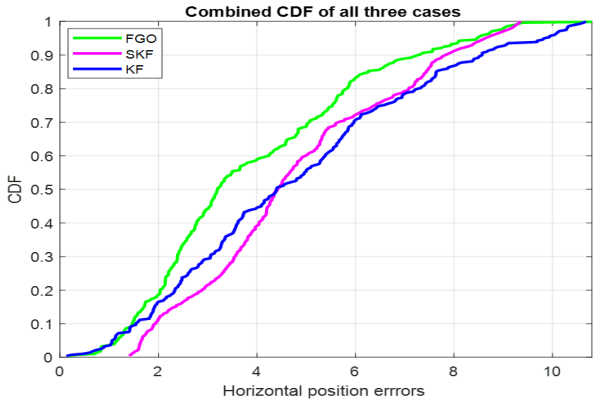

Fig. 9. Overall cdf of horizontal positioning errors from all three cases.

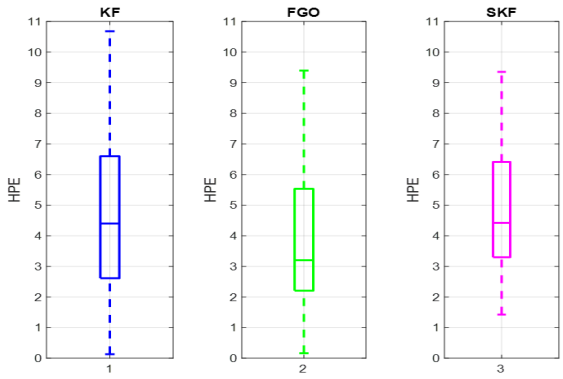

Fig. 10. Overall box plots from three cases.

B. Analysis of Improvement in FGO Versus Different Pedestrians and Motions

1) FGO Improvement Over Motions: It becomes necessary to assess the impact of these types of motions on the performance of FGO. The positioning performance of FGO over these two motions of the different pedestrians is detailed in Table II and visually represented in the box-and-whisker plot in Fig. 11. From the results, it can be noted that, overall, the performance of FGO is better than that of KF. In both motions, FGO gets lower errors compared to KF. We can also see that the results of walking motion are better compared to running motion, and this is because the PDR model is better adapted to that type of motion. The improvement of FGO is quite consistent over the two motions and different statistics Table II: around 25% for the mean error, around 30% for the median error, and around 25% for the 90th percentiles. However, there is an improvement in the standard deviation for walking motion of only around 6%, but we can see a negative improvement in running motion, which means that

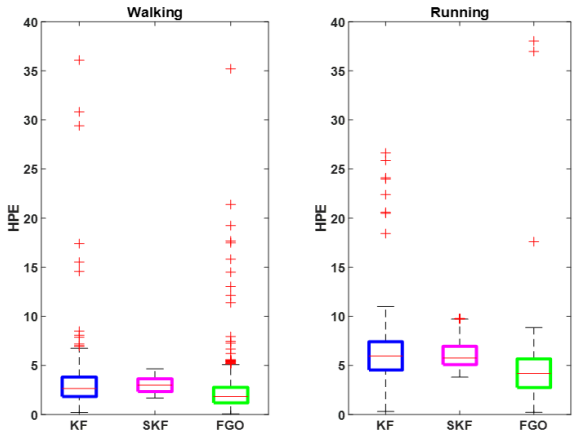

Fig. 11. Box plots illustrating the performance distribution of FGO (green box), SKF (magenta box), and KF (blue box) in PDR-GNSS fusion for walking and running motions.

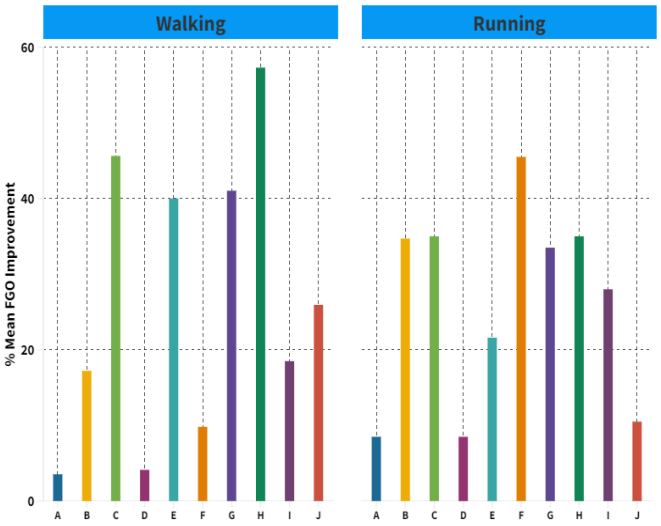

Fig. 12. Comparative analysis of 2-D mean position error via FGO versus KF for walking and running for different pedestrians (A-J).

the dispersion of the errors seems similar for both fusion methods. This is due to the diverse involvement of pedestrians, variations in gait cycles, and differing heights, all of which contribute to the variability observed in the FGO standard deviation for running motion.

2) FGO Improvement Over Users: Human gait dynamics differ due to differences in walking pattern, gender, and height, and the performance of individual PDR blocks is influenced by these aspects. As mentioned earlier, developing a flexible step detector, step length estimator, and heading estimator for diverse pedestrians poses a significant challenge. Consequently, no matter how diverse users' walking patterns and attributes align with the implemented PDR models, the standard deviation in the preceding boxplot did not improve for running motion. We can see in Fig. 12 that the actual improvement of FGO varies a lot for different users.

3) General FGO Improvement: To characterize the overall improvement of FGO over KF, we compare their 2-D mean position errors while taking into consideration the performance of PDR for each individual and motion type. However, the PDR's performance is determined by the individual performance of its main components: the step detector, the step length estimator, and the step heading estimator. Since we

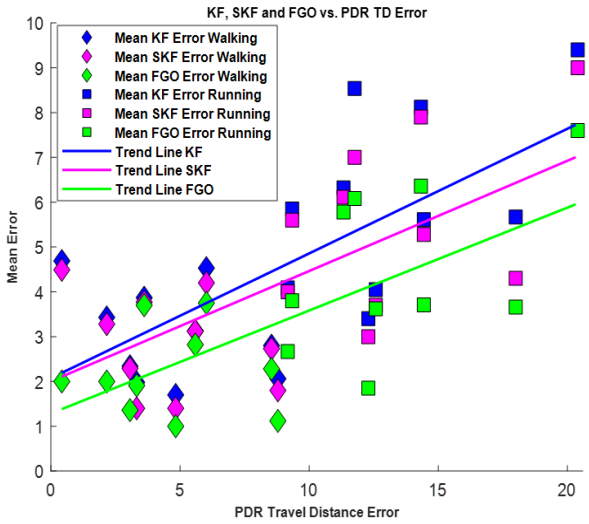

Fig. 13. Comparison of 2-D mean positioning errors between KF, SKF, and FGO with PDR travel distance error. The KF performance is depicted by the blue trend line and SKF by the magenta line, while the FGO performance is represented by the green trend line.

do not have the ground truth of these individual components, we considered the PDR travel distance as a proxy of it. It can be seen the individual mean error points and two regression lines from both fusion algorithms in Fig. 13. These mean error points are categorized by the type of motion and fusion algorithm.

From Fig. 13, it can be observed that FGO consistently shows lower mean error values compared to KF for each pedestrian and both motion types, regardless of the PDR performance value. Moreover, it can also be seen that the FGO regression line is more flatter than KF. However, the difference between the two regression lines increases as the PDR performance gets worse. We can measure that with the slope of the lines by $y = mx + b$, which gives us the slope for the KF regression line, which is 0.27823, and the FGO trend line is 0.22964. These results highlight that FGO gets lower errors and is somewhat more robust against bad PDR performances.

It is difficult to compare the obtained results to the ones reported by prior studies because of the different types of experiments. The study in [10] evaluated FGO for PDR-GNSS fusion with single walking motion data in the open sky environment. Meanwhile, a study [11] examined nine different datasets in urban environments with different smartphone positionings, such as box, pocket, and handheld. Our experiments are different from those presented in these studies as we analyzed the performance of FGO against KF and SKF under different PDR errors arising from transient variations in the way a smartphone is carried and due to different motions, heights, and gender (walking and running, and ten different pedestrians). Nevertheless, the trends and behaviors of FGO are coherent in all articles.

In FGO, all historical information is considered during the optimization, and the overall performances are improved gradually, exhibiting the capability to effectively mitigate errors associated with PDR data. As a result, despite the bad performance of the PDR block, FGO consistently outperformed KF. Implementing real PDR systems that

TABLE II
FGO IMPROVEMENT AGAINST KF AND SKF FOR PDR-GNSS FUSION ARCHITECTURE

Motion	**Mean**				**Median**			
	KF	FGO	SKF	% (KF and SKF)	KF	FGO	SKF	% (KF and SKF)
Walking	3.0325	2.2434	3.0120	26.06 and 25.00	2.6483	1.8479	3.0710	30.25 and 39.82
Running	6.1233	4.6483	6.0011	24.04 and 22.30	5.9661	4.1786	5.5001	30.00 and 25.40
Motion	**STD**				**90th Percentile**			
	KF	FGO	SKF	% (KF and SKF)	KF	FGO	SKF	% (KF and SKF)
Walking	2.3984	2.2655	0.674	5.56 and - 70.00	5.0441	3.9103	3.878	22.47 and - 0.01
Running	2.9973	3.1459	1.350	-4.78 and -57.00	9.2437	6.8397	8.4200	25.99 and 18.00

generalize well over different pedestrians, FGO appears to be a superior choice compared to KF.

VI. CONCLUSION AND FUTURE WORK

The performance of FGO has been investigated for the GNSS outliers in INS-GNSS fusion systems. However, its performance in the PDR + GNSS fusion architecture in a pedestrian navigation context was not investigated under the different PDR outliers. Therefore, this article provides a thorough comparison of FGO over KF for PDR-GNSS fusion in smartphones, taking into account the impact of PDR performance in the fusion using a real dataset collected at the football field. In this research, PDR errors are comprised of two main sources: on the one hand, the transients in the way the smartphone is carried; on the other hand, the different gait dynamics of pedestrians. Since FGO is well known for mitigating the impact of GNSS outliers in INS-GNSS fusion architectures, similarly, it has been observed that FGO mitigates the impact of the PDR errors formed by SHEs and CLEs in the PDR-GNSS fusion architectures. Based on the analysis findings, the enhanced performance of FGO compared to KF can be attributed to multiple iterations and the utilization of historical measurements. Opting for FGO seems more favorable when deploying practical PDR systems designed to work effectively across diverse pedestrians.

Despite FGO's effective performance in mitigating the impact of PDR errors in smartphone-based PDR-GNSS fusion, its batch-style fusion is impractical for real-time applications. Incorporating historical measurements raises computation costs, and considering that pedestrians have a limited pace, there is no necessity to involve all measurements in the fusion process. Instead, it can be implemented with a window of a few previous measurements. Future work could focus on the following aspects:

1) impact of different window sizes on the improvements of FGO over traditional fusion algorithms;
2) the tradeoff between the accuracy and computational load of FGO.

Overall, our assessment leads us to conclude that FGO-based sensor fusion holds significant promise as a prospective alternative to KF-based approaches in the forthcoming decades.

REFERENCES

[1] F. Zangenehnejad and Y. Gao, "GNSS smartphones positioning: Advances, challenges, opportunities, and future perspectives," *Satell. Navigat.*, vol. 2, no. 1, pp. 1–23, Nov. 2021.

[2] P. D. Groves, "Principles of GNSS, inertial, and multisensor integrated navigation systems, 2nd edition [book review]," *IEEE Aerosp. Electron. Syst. Mag.*, vol. 30, no. 2, pp. 26–27, Feb. 2015.

[3] W. Yan, L. Bastos, A. Magalhães, Y. Zhang, and A. Wang, "Assessing Android smartphone based GNSS positioning accuracy," in *Proc. China Satell. Navigat. Conf. (CSNC)*. Singapore: Springer, 2020, pp. 144–153.

[4] J. Hu, D. Yi, and S. Bisnath, "A comprehensive analysis of smartphone GNSS range errors in realistic environments," *Sensors*, vol. 23, no. 3, p. 1631, Feb. 2023.

[5] U. Robustelli, V. Baiocchi, and G. Pugliano, "Assessment of dual frequency GNSS observations from a Xiaomi Mi 8 Android smartphone and positioning performance analysis," *Electronics*, vol. 8, no. 1, p. 91, Jan. 2019.

[6] G. Falco, M. Pini, and G. Marucco, "Loose and tight GNSS/INS integrations: Comparison of performance assessed in real urban scenarios," *Sensors*, vol. 17, no. 2, p. 255, Jan. 2017.

[7] A. Angrisano et al., "GNSS/INS integration methods," Ph.D. thesis, Dipartimento di Scienze Applicate, Universita'degli Studi di Napoli PARTHENOPE, Naples, Italy, 2010, vol. 21.

[8] J. A. Farrell and J. Wendel, "GNSS/INS integration," in *Springer Handbook of Global Navigation Satellite Systems*. Cham, Switzerland: Springer, 2017, pp. 811–840.

[9] D. Titterton and J. L. Weston, *Strapdown Inertial Navigation Technology*, vol. 17. Edison, NJ, USA: IET, 2004.

[10] C. Jiang et al., "Implementation and performance analysis of the PDR/GNSS integration on a smartphone," *GPS Solutions*, vol. 26, no. 3, p. 81, Jul. 2022.

[11] C. Jiang et al., "Smartphone PDR/GNSS integration via factor graph optimization for pedestrian navigation," *IEEE Trans. Instrum. Meas.*, vol. 71, 2022, Art. no. 8504112, doi: 10.1109/TIM.2022.3186082.

[12] Y. Zhong, W. Wen, and L.-T. Hsu, "Trajectory smoothing using GNSS/PDR integration via factor graph optimization in urban canyons," 2022, *arXiv:2212.14264*.

[13] A. Rehman, H. Shahid, M. A. Afzal, and H. M. A. Bhatti, "Accurate and direct GNSS/PDR integration using extended Kalman filter for pedestrian smartphone navigation," *Gyroscopy Navigat.*, vol. 11, no. 2, pp. 124–137, Apr. 2020.

[14] H. Lan, C. Yu, and N. El-Sheimy, "An integrated PDR/GNSS pedestrian navigation system," in *Proc. China Satell. Navigat. Conf. (CSNC)*, vol. 3. Berlin, Germany: Springer, 2015, pp. 677–690.

[15] F. Dellaert and M. Kaess, "Factor graphs for robot perception," *Found. Trends Robot.*, vol. 6, nos. 1–2, pp. 1–139, 2017.

[16] D. Koller and N. Friedman, *Probabilistic Graphical Models: Principles and Techniques*. Cambridge, MA, USA: MIT Press, 2009.

[17] W. Li, X. Cui, and M. Lu, "A robust graph optimization realization of tightly coupled GNSS/INS integrated navigation system for urban vehicles," *Tsinghua Sci. Technol.*, vol. 23, no. 6, pp. 724–732, Dec. 2018.

[18] W. Wen, X. Bai, Y. C. Kan, and L.-T. Hsu, "Tightly coupled GNSS/INS integration via factor graph and aided by fish-eye camera," *IEEE Trans. Veh. Technol.*, vol. 68, no. 11, pp. 10651–10662, Nov. 2019.

[19] W. Wen, T. Pfeifer, X. Bai, and L.-T. Hsu, "Comparison of extended Kalman filter and factor graph optimization for GNSS/INS integrated navigation system," 2020.

[20] W. Wen, Y. C. Kan, and L.-T. Hsu, "Performance comparison of GNSS/INS integrations based on EKF and factor graph optimization," in *Proc. 32nd Int. Tech. Meeting Satell. Division Inst. Navigat. (ION GNSS)*, Oct. 2019, pp. 3019–3032.

[21] Q. Li, L. Zhang, and X. Wang, "Loosely coupled GNSS/INS integration based on factor graph and aided by ARIMA model," *IEEE Sensors J.*, vol. 21, no. 21, pp. 24379–24387, Nov. 2021.

[22] S. Xin, X. Wang, J. Zhang, K. Zhou, and Y. Chen, "A comparative study of factor graph optimization-based and extended Kalman filter-based PPP-B2b/INS integrated navigation," *Remote Sens.*, vol. 15, no. 21, p. 5144, Oct. 2023.

[23] N. Boguspayev, D. Akhmedov, A. Raskaliyev, A. Kim, and A. Sukhenko, "A comprehensive review of GNSS/INS integration techniques for land and air vehicle applications," *Appl. Sci.*, vol. 13, no. 8, p. 4819, Apr. 2023.

[24] C. Jiang et al., "Cooperative smartphone GNSS/PDR for pedestrian navigation," *IEEE Trans. Circuits Syst. II, Exp. Briefs*, vol. 70, no. 6, pp. 2301–2305, Jun. 2023.

[25] C. Jiang, Y. Chen, C. Chen, and J. Hyyppä, "Walking gaits aided mobile GNSS for pedestrian navigation in urban areas," *IEEE Internet Things J.*, vol. 11, no. 5, pp. 8499–8510, Mar. 2024.

[26] A. Hussain and L. E. Díez, "Comparison of FGO and KF for PDR-GNSS fusion on smartphone for diverse pedestrian movements," in *Proc. 13th Int. Conf. Indoor Positioning Indoor Navigat. (IPIN)*, Sep. 2023, pp. 1–6.

[27] H. E. Rauch, F. Tung, and C. T. Striebel, "Maximum likelihood estimates of linear dynamic systems," *AIAA J.*, vol. 3, no. 8, pp. 1445–1450, Aug. 1965.

[28] A. Rehman et al., "PDR/GNSS fusion algorithm based on joint heading estimation," in *Proc. China Satell. Navigat. Conf. (CSNC)*, vol. 1. Singapore: Springer, 2019, pp. 326–339.

[29] X. Tao, X. Zhang, F. Zhu, F. Wang, and W. Teng, "Precise displacement estimation from time-differenced carrier phase to improve PDR performance," *IEEE Sensors J.*, vol. 18, no. 20, pp. 8238–8246, Oct. 2018.

[30] R. Zhang, J. Mi, J. Li, and Q. Wang, "A continuous PDR and GNSS fusing algorithm for smartphone positioning," *Remote Sens.*, vol. 14, no. 20, p. 5171, Oct. 2022.

[31] X. Wu, B. Xiao, C. Wu, Y. Guo, and L. Li, "Factor graph based navigation and positioning for control system design: A review," *Chin. J. Aeronaut.*, vol. 35, no. 5, pp. 25–39, May 2022.

[32] F. Dellaert, "Factor graphs and GTSAM: A hands-on introduction," Georgia Inst. Technol., Atlanta, GA, USA, Tech. Rep. GT-RIM-CP&R-2012-002, 2012.

[33] V. Indelman, S. Williams, M. Kaess, and F. Dellaert, "Information fusion in navigation systems via factor graph based incremental smoothing," *Robot. Auto. Syst.*, vol. 61, no. 8, pp. 721–738, Aug. 2013.

[34] D. Chen and G. X. Gao, "Probabilistic graphical fusion of LiDAR, GPS, and 3D building maps for urban UAV navigation," *NAVIGATION*, vol. 66, no. 1, pp. 151–168, Jan. 2019.

[35] T. Pfeifer and P. Protzel, "Expectation-maximization for adaptive mixture models in graph optimization," in *Proc. Int. Conf. Robot. Autom. (ICRA)*, May 2019, pp. 3151–3157.

[36] S. Bhamidipati and G. X. Gao, "Multiple GPS fault detection and isolation using a graph-SLAM framework," in *Proc. Int. Tech. Meeting Satell. Division Inst. Navigat.*, Oct. 2018, pp. 2672–2681.

[37] J. Huang and F. Wu, "A study on the use of graph signal processing techniques for satellite-based navigation systems," in *Proc. Int. Tech. Meeting Inst. Navigat.*, 2016, pp. 448–455.

[38] R. M. Watson and J. N. Gross, "Evaluation of kinematic precise point positioning convergence with an incremental graph optimizer," in *Proc. IEEE/ION Position, Location Navigat. Symp. (PLANS)*, Apr. 2018, pp. 589–596.

[39] G. Guo, R. Chen, X. Niu, K. Yan, S. Xu, and L. Chen, "Factor graph framework for smartphone indoor localization: Integrating data-driven PDR and Wi-Fi RTT/RSS ranging," *IEEE Sensors J.*, vol. 23, no. 11, pp. 12346–12354, Jun. 2023.

[40] R. M. Watson and J. N. Gross, "Robust navigation in GNSS degraded environment using graph optimization," in *Proc. 30th Int. Tech. Meeting Satell. Division Inst. Navigat. (ION GNSS)*, 2017, pp. 2906–2918.

[41] T. Pfeifer and P. Protzel, "Robust sensor fusion with self-tuning mixture models," in *Proc. IEEE/RSJ Int. Conf. Intell. Robots Syst. (IROS)*, Oct. 2018, pp. 3678–3685.

[42] W. Wen, T. Pfeifer, X. Bai, and L.-T. Hsu, "It is time for factor graph optimization for GNSS/INS integration: Comparison between FGO and EKF," 2020, *arXiv:2004.10572*.

[43] W. Wen, L.-T. Hsu, and G. Zhang, "Performance analysis of NDT-based graph SLAM for autonomous vehicle in diverse typical driving scenarios of Hong Kong," *Sensors*, vol. 18, no. 11, p. 3928, Nov. 2018.

[44] X. Li, H. Yu, X. Wang, S. Li, Y. Zhou, and H. Chang, "FGO-GIL: Factor graph optimization-based GNSS RTK/INS/LiDAR tightly coupled integration for precise and continuous navigation," *IEEE Sensors J.*, vol. 23, no. 13, pp. 14534–14548, Jul. 2023.

[45] H. Weinberg, "Using the ADXL202 in pedometer and personal navigation applications," Analog Devices, Wilmington, MA, USA, Appl. Note AN-602, 2002, vol. 2, no. 2, pp. 1–6.

[46] H. P. Gavin, "The Levenberg–Marquardt algorithm for nonlinear least squares curve-fitting problems," Dept. Civil Environ. Eng., Duke Univ., Durham, NC, USA, 2019, vol. 19.

[47] A. R. Jiménez, F. Seco, and J. Torres-Sospedra, "Tools for smartphone multi-sensor data registration and GT mapping for positioning applications," in *Proc. Int. Conf. Indoor Positioning Indoor Navigat. (IPIN)*, 2019, pp. 1–8.

Amjad Hussain Magsi received the B.E. degree in electronic engineering and the master's degree in electronic systems engineering from the Mehran University of Engineering Technology, Jamshoro, Pakistan, in 2017 and 2022, respectively. He is currently pursuing the Ph.D. degree in engineering for the information society and sustainable development under the supervision of Luis Enrique Díez Blanco with the University of Deusto, Bilbao, Spain.

During his bachelor's, he was an Erasmus Scholar at the University of Limerick, Limerick, Ireland. From 2019 to 2022, he worked as a Lab Engineer at Dawood University of Engineering and Technology, Karachi, Pakistan. He is also working at the Deusto Smart Mobility Research Team, University of Deusto. His research interests include data fusion for developing location-based services, smartphone positioning, factor graph optimization, and machine learning theory and algorithms for localization and intelligent environments.

Luis Enrique Díez received the bachelor's degree in telecommunications engineering from the University of Deusto, Bilbao, Spain, in 2005, the master's degree in communications technologies and systems from the Telecommunications Engineering School, Polytechnic University of Madrid, Madrid, Spain, in 2012, and the Ph.D. degree in engineering from the University of Deusto in 2019.

From 2005 to 2011, he worked at Everis, Madrid, as a Senior IT Consultant. From 2013 to 2014, he was with the SOFTLAB Research Group, Carlos III University of Madrid (UC3M), Madrid, as a Research Support Technician. From 2014 to 2022 he worked as a Researcher at DeustoTech, the Research Institute of the Engineering Faculty, University of Deusto. He currently works as an Assistant Professor at the Faculty of Engineering, University of Deusto, and he is a member of the research group "Deusto Smart Mobility." He has worked (leading some of them) on more than ten regional, national, and international research projects and contracts. He has co-authored 15 research manuscripts published in international journals and more than ten communications at international congresses. His research interests include signal processing and data fusion for the development of location-based services, ambient assisted living, and intelligent environments.